agriculture

Article

Process Analysis and Parameters Optimization of Black Soldier Fly Sand Mixture with Two-Stage Sieve Surface Vibration Separating Machine

Shisheng Song [1], Yushi Wang [1], Ting Zhou [1], Songlin Sun [1], Yulong Yin [2] and Caiwang Peng [1,*]

[1] College of Mechanical and Electrical Engineering, Hunan Agricultural University, Changsha 410128, China
[2] College of Animal Science and Technology, Hunan Agricultural University, Changsha 410128, China
* Correspondence: hnndpcw@hunau.edu.cn

Abstract: The application of the conventional vibrating screen to the separation of the black soldier fly (BSF) sand mixture has several problems (e.g., high rate of impurity and low efficiency). A two-stage sieve surface vibratory sorting device with combined planar and curved surfaces was investigated, and its critical operating parameters were determined. Moreover, a coupling simulation model of the sieve surface and the larvae–sand mixture was built based on the characteristics of the BSF breeding process, and its critical operating parameters were optimized. Next, the Plackett–Burman test was set to determine the significant factors for the separation of two-stage sieve surface vibrations as amplitude and curved height. The process of crushing separation of frass aggregates and the process of collision transport of BSF larvae were studied through simulation, and the actual test stand was built for parameter verification tests. The preferred parameter combinations comprised 0.012 m amplitude and 0.007 m curved surface height at the impurity rate of 2.34% and the insect injury rate of 5.65%, as well as 0.013 m amplitude and 0.005 m curved surface height at the impurity rate of 3.15% and the insect injury rate of 4.3%, respectively, thus conforming to the requirement of separating BSF larvae–sand mixture to reduce the impurity and prevent larvae injury. The results of this study can lay a basis for the structural improvement and operational parameter adjustment of the BSF larvae–sand mixture separation device.

Keywords: black soldier fly; combined sieve surface; EDEM; vibration separation; parameters optimization

Citation: Song, S.; Wang, Y.; Zhou, T.; Sun, S.; Yin, Y.; Peng, C. Process Analysis and Parameters Optimization of Black Soldier Fly Sand Mixture with Two-Stage Sieve Surface Vibration Separating Machine. *Agriculture* **2022**, *12*, 2099. https://doi.org/10.3390/agriculture12122099

Academic Editors: Eugenio Cavallo, Carlo Bisaglia and Francesco Marinello

Received: 26 October 2022
Accepted: 6 December 2022
Published: 8 December 2022

1. Introduction

Kitchen waste is currently increasing as people's living standards have been increasingly improved. Most kitchen waste has been in landfills, taking up considerable space, and its leachate overflow seriously jeopardizes the environment [1–3]. Since kitchen waste has high water content and abundant organic matter, the application of decaying resource insects to bio-transform kitchen waste and achieve resource utilization has become a research hotspot [4–6].

The black soldier fly, *Hermetia illucens* (Diptera: Stratiomyidae), takes on a great significance since its larvae are capable of encouraging the recycling of organic waste and kitchen waste by feasting on organic materials originating from plants, animals, and humans. The degradation rate of organic matter can reach nearly 70% [7–9], and the transformed BSF sand can serve as organic fertilizer. Prepupae BSF, containing 40% protein [10–12], can be fed to pigs [13] and fish [14] as protein feed, with significant economic rewards [15,16]. To maximize resource utilization, the BSF sand mixture (the black soldier fly larvae (BSFL) and the BSF organic fertilizer) should be rapidly separated before the pupation of larvae.

Extensive studies have been conducted on screening. Dong et al. [17] explored the variables that affect the efficiency of linear vibrating screens for screening coal particles using the discrete element method. To be specific, the entirety comprises considerable discrete individuals, whereas there are two forms of dependence and dispersion between individuals that can be adopted to analyze and solve the dynamics of complex systems. Li et al. [18] investigated the effect of vibration parameters on particle delamination and sieve penetration based on DEM (discrete element method) numerical simulation. They also proposed the concept of penetration probability. Zhou et al. [19] have noted that the "Hertz–Mindlin with JKR" model can accurately simulate the sieving process of wet particles by simulating the sieving of damp sand and gravel using the JKR model. To be specific, JKR model refers to a contact model with cohesive force between particles, introducing the concept of surface energy to characterize the magnitude of inter-particle adhesion. Ma et al. [20] designed a concave–convex non-smooth sieve surface based on the viscosity-reducing properties of the bionic non-smooth plane, which revealed the intrinsic principle of viscosity reduction and desorption of the sieve surface. However, there has been limited numerical simulation research on the separation of insect–frass. BSF sand separation comprises light separation, thermal separation, electric stimulation separation, etc. The above procedures primarily use the biological properties of the BSF to separate it from the base material, which poses fewer hazards to the BSFL. However, its lengthy separation time, subpar separation efficiency, expensive cost, and limited actual application scale all combine against it. The mechanical separation approach only uses mechanical means to separate the larvae from the frass particles. Given the features of BSF sand, Fang et al. [21] well separated the BSFL from the BSF sand with the water content of 30.2% using a sieve-hole segmented trommel screen. Nevertheless, since the BSF sand mixture has certain water content and organic fertilizer particles that exhibit a bonding phenomenon, the vibration separation effect of frass, only relying on the conventional sieve surface, is poor; the larger the rate of impurity, the higher the rates of larval damage and poor targeting will be. Based on the above background, a two-stage sieve surface combination vibration device was designed in the earlier stage, dividing the sieve surface into two sections in accordance with the difference in separation objects. This device is capable of separating larvae–sand mixture, whereas there has been rare research on the optimization of parameters in the process of two-stage sieve surface vibration separation of BSF sand mixture.

In brief, based on the authors' existing research [22–24], the characteristics of BSF breeding and the characteristics of larvae–frass mixture were combined, a model of frass aggregates and BSFL was constructed, and discrete element simulation was performed to identify the fundamental trends of velocity change and mechanical change features in the separation process. The experimental purpose of this study was to reduce the rate of impurity and insect injury. Moreover, the optimal combination of parameters was obtained, thus further optimizing the parameters of the two-stage screen surface vibration separation device, increasing the cleaning rate, and enhancing the parameter adaptability of the separation device to the BSF sand mixture.

2. Materials and Methods

2.1. Separation Process of Black Soldier Fly Sand

By transforming organic substances other than carbon and nitrogen from kitchen waste into the larval organic matter, on the one hand, and retaining them in the larval residue, on the other, BSFL can treat kitchen waste efficiently and safely, reduce kitchen waste, safely utilize the resource of kitchen waste, and produce high-value products [25,26]. Four-day-old BSFL were placed in the kitchen waste, and high-protein BSFL and high-fertility organic fertilizer were obtained by feeding during the over-belly treatment. Subsequently, BSFL sand mixture was transferred and transported from the breeding trays that employed equipment (e.g., bucket–wheel mechanisms) before the separation process [22]. The separating equipment is a vital part of the process and can directly affect the utilization degree of the BSFL sand mixture, as shown in Figure 1.

Figure 1. Collection and sorting process of black soldier fly sand mixture.

For the distribution law of "more in the front and less in the back" of fine particles under the screen, based on the improvement and optimization of the previous research [21], the sieve surface is divided into two stages, as shown in Figure 2. Separation part of the front surface screen: Frass aggregates and the majority of BSFL entering the pre-pupal stage remain on the sieve surface and slide backward with the screen under the action of the vibrating screen, while fine frass particles and a limited number of slowly growing infantile BSFL are separated through the front plane surface. Separation part of the back curved screen: The BSFL and frass agglomerates are thrown from the crest of the curved screen to the trough by the action of the curved screen, and under the coupling force of shear and impact of the surface, the frass agglomerates are broken and depolymerized into fine particles, while the BSFL cannot penetrate the screen and continue to move toward the back end of the screen, and the BSF sand mixture gradually separates. Considerable fine particles of frass are obtained in the under-screen collection box, while a small amount of frass is obtained in the collection box at the end of the discharge, and the BSFL with a minor trash rate is obtained in the collection box at the tail-end discharge.

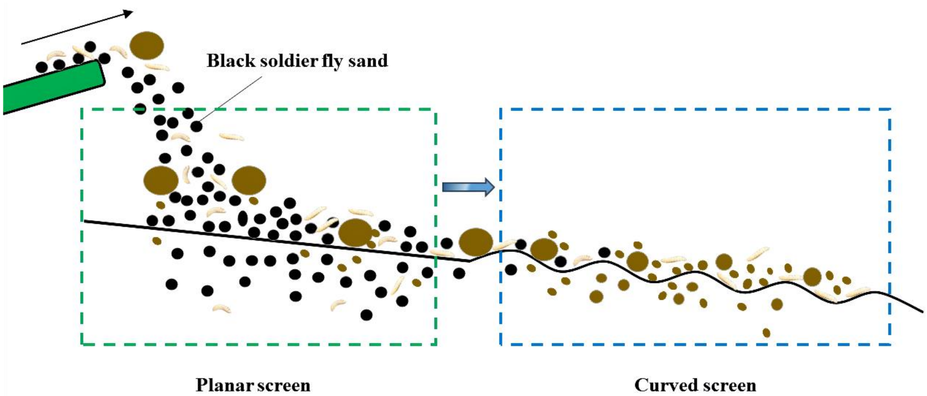

Figure 2. Schematic diagram of two-stage sieve surfaces separation.

2.2. Analysis of Shape and Size of Frass Aggregates

The macroscopic outline of frass aggregates, which are granular cohesive BSF organic fertilizer particles that do not contain BSFL, is typically portrayed by three mutually perpendicular axes, the long axis, the middle axis, and the short axis, which indicate the length, width, and thickness of the frass aggregates, respectively. The length is the maximum dimension of the plane projection figure, the width refers to the maximum dimension perpendicular to the length direction, and the thickness refers to the linear dimension perpendicular to the length and width direction. A total of 100 BSF frass aggregates were randomly selected to measure their triaxial size with a digital vernier caliper with an accuracy of 0.00001 m. The distribution of triaxial size is shown in Figure 3, and the triaxial size of BSF frass aggregates follows a normal distribution.

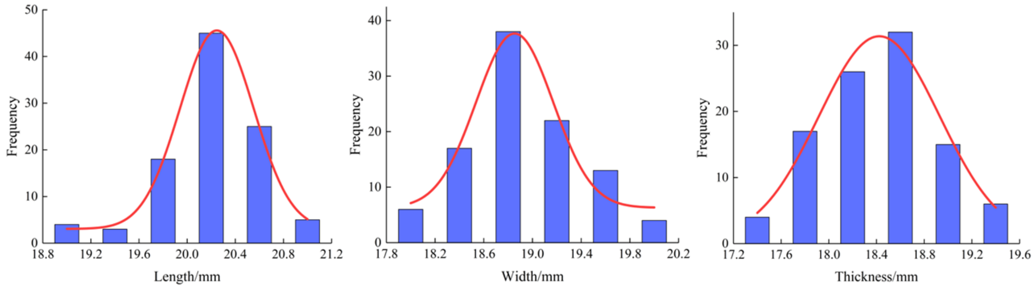

Figure 3. Triaxial size distribution of BSF frass aggregates.

Figure 4 presents the triaxial dimensions relationship of the frass aggregates. As depicted in the figure, the linear correlation between the length–width and length–thickness of the frass aggregates was significantly greater than that between the width–thickness. As a result, the length can be considered the primary dimension, the width and thickness as the secondary dimensions. The theoretical width (W′) and thickness (T′) of the respective frass aggregate were calculated separately using the relational equations in Figure 4 and compared with the actual frass aggregate width (W) and thickness (T) (Table 1). As depicted in Table 1, the gap between the theoretical values of width and thickness and the actual values was small. Thus, the length can serve as the primary dimension and generated in accordance with the normal distribution for building the particle swarm model of insect manure agglomeration, and the secondary dimension can be calculated based on the relation equation with the primary dimension; the particle population generated using this method was closer to the actual situation in both shape and size distribution. To save the computation and shorten the simulation time, the agglomerate models were set as spheres with a diameter of 0.02 m according to the agglomerate size distribution in Figure 3, and generated a total of 100 agglomerate models in the simulation test.

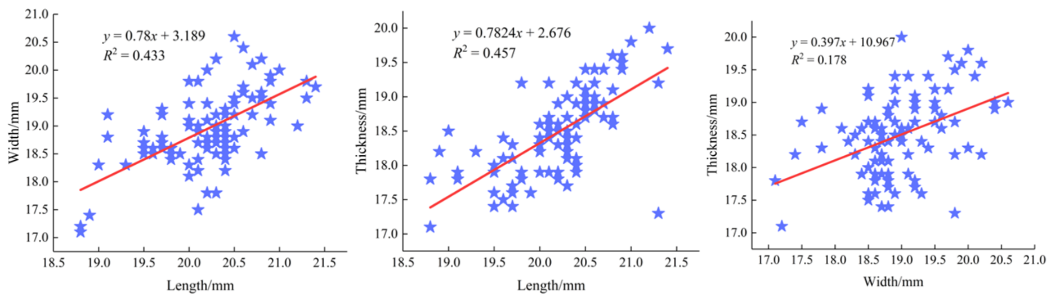

Figure 4. Scatter plot of the relationship between the triaxial dimensions of the frass aggregates.

Table 1. Comparison of theoretical and actual sub-dimensions.

Project	W′/m	T′/m	W/m	T/m	(W−W′)/W%	(T−T′)/T%
AVG	0.0185	0.0179	0.0189	0.0183	2.44	2.37
S.D.	0.006	0.006	0.007	0.006	3.06	1.85

2.3. Discrete Element Modeling of Black Soldier Fly Sand

2.3.1. Agglomerate Contact Modeling

The sieve surface, the frass agglomerates, and the BSFL were treated as three types of moving bodies with different kinetic characteristics. The curved sieve surface was generally rigid; frass agglomerates were characterized by excitation and disaggregation; the BSFL exhibited some viscoelasticity on the polypide surface; and the coupling effects of the three were complex. Accordingly, it is of high application value to investigate the movement characteristics and velocity variation patterns of frass aggregates and BSFL on the surface of the curved screen to clarify the effects of each separation parameter on the agglomeration–disaggregation regularity and collision characteristics of BSFL, respectively [27].

When the frass agglomerates came into contact with the sieve, the existence of approach velocity between the respective particles inside the agglomerates caused the extrusion collision between the particles; since the frass agglomerates contain certain water, the liquid bridge between the particles significantly affected the relative motion between the particles, and the "Hertz–Mindlin with Bonding" model in the discrete element method better simulated this bonding constraint between the wet particles [28]. The interparticle bonding constraint comprises springs uniformly distributed in the region between two particles, which exhibit constant normal and tangential stiffness; when the distance between the centers of mass of the two particles is not greater than the sum of the bond radii of the two particles, a bonding constraint is generated between the particles, which can transmit not only forces but also moments [29].

The contact model of the frass particles is illustrated in Figure 5. The resultant force generated by the bonding constraint between the particles was located at the center of the interface where the two spheres intersected, and the resultant force was divided into the tangential and normal components as follows:

$$\delta F_b^n = -k_b^n A \delta t \tag{1}$$

$$\delta F_b^s = -k_b^s A \delta t \tag{2}$$

$$\delta M_b^n = -\omega_n k_b^n J \delta t \tag{3}$$

$$\delta M_b^s = -\omega_s k_b^s J \delta t \tag{4}$$

where A denotes the contact area, $A = \pi R_b^2$, in m^2; J represents the rotational inertia, $J = \frac{1}{2}\pi R_b^4$, in m^4; R_b expresses the bond radius, in m; δt is the time step, in s; $M_b^{n,s}$ is the normal or tangential moment, in N/m; $\omega_{n,s}$ is the normal or tangential angular velocity of the particle, in rad/s; and $K_b^{n,s}$ is the normal or tangential stiffness, in N/m.

In the normal direction according to the principle of maximum tensile stress, when the maximum tensile stress σ_{max} in the bond constraint is greater than the tensile strength R_m, the bond constraint fails, and the model is broken, which is written as follows:

$$\sigma_{max} > R_m = \frac{-F_b^n}{A} + \frac{2M_b^s}{J} \cdot R_b \tag{5}$$

In the tangential direction, in accordance with the Mohr–Coulomb criterion, when the maximum shear stress τ_{max} in the bond restraint is greater than the shear strength f, the bond restraint is destroyed by shear, which is expressed as follows:

$$\tau_{max} > f = \frac{F_b^s}{A} + \frac{M_b^n}{J} \cdot R_b \tag{6}$$

When the particles come into contact with each other, under the effect of the bond constraint stiffness, forces and torques will be produced in the region between the particles. When the maximum tangential or normal stress between the particles either generated to meet Equations (5) or (6), the bond constraint fracture, while removing the accompanying forces and moments, the particles slip separation, separation processes with an increase in particle spacing, the inter-particle liquid bridge is stretched until fracture and particle aggregation broken depolymerization. The tumbling and crushing process of the aggregates refers to the transformation of the frass aggregates from a continuous medium model to a discrete medium model.

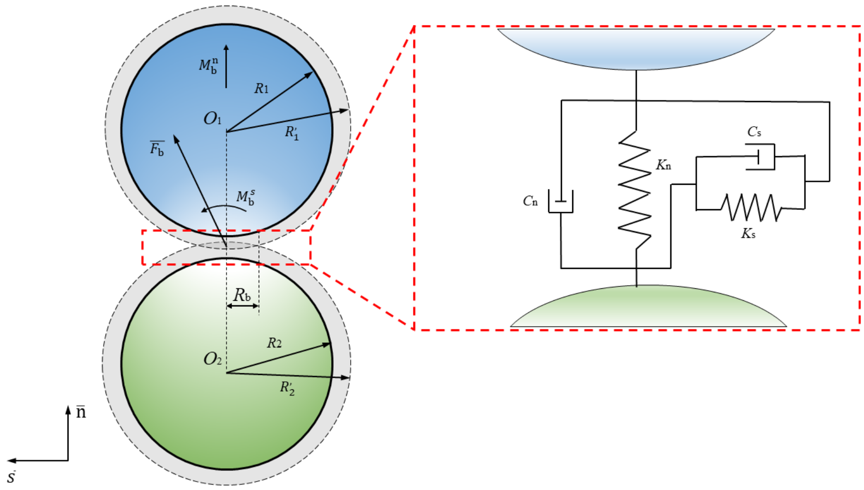

Figure 5. Contact model between frass particles.

2.3.2. Calibration of Agglomerate Bonding Parameters

Besides the material intrinsic parameters and inter-material contact parameters, the material bonding parameters should be calibrated [23,30], which comprise normal stiffness coefficient, tangential stiffness coefficient, critical normal stress, critical tangential stress, and bonding radius. To be specific, the bonding radius of frass particles are written as follows:

$$\frac{m_1}{m_1+m_2} = \frac{\rho_1 V_1}{\rho_1 V_1+\rho_2 V_2} \tag{7}$$

$$V_1 = \frac{4}{3}\pi R_b^3 - \frac{4}{3}\pi R^3 \tag{8}$$

$$V_2 = \frac{4}{3}\pi R^3 \tag{9}$$

where m_1 and m_2 denote the masses of water and frass particles, in kg; ρ_1 and ρ_2 represent the densities of water and frass particles, in kg/m^3; V_1 and V_2 express the volumes occupied by water and frass particles, in m^3; W is the moisture content of frass aggregates, %; R is the radius of frass particles, in m.

Substituting ρ_1 = 1000 kg/m^3, ρ_2 = 2000 kg/m^3, W = 12.5% and R = 0.0012 m into Equations (7)–(9), can obtain the contact radius R_b = 0.0013 m of frass particles. Based on the bonding theory, the normal stiffness coefficient and tangential stiffness coefficient of frass aggregates are:

$$r_n = \frac{4}{3}\left(\frac{1-\mu_1^2}{E_1} + \frac{1-\mu_2^2}{E_2}\right)^{-1} \cdot \left(\frac{R_1+R_2}{R_1 R_2}\right)^{-\frac{1}{2}} \tag{10}$$

$$r_s = \left(\frac{1}{2} \sim \frac{2}{3}\right) r_n \tag{11}$$

$$G = \frac{E}{2+2\mu} \tag{12}$$

where r_n denotes the normal stiffness coefficient, in N/m; μ_1 and μ_2 represent the Poisson's ratios of particles 1 and 2, respectively; E_1 and E_2 are the elastic moduli of particles 1 and 2, in Pa; R_1 and R_2 are the radii of particles 1 and 2, respectively, in m; r_s expresses the tangential stiffness coefficient, in N/m; G is the shear modulus of particles, in Pa. Since the material of the particles in this study is BSFL frass, the values of the respective parameter of the particles are the same, putting the values of $\mu_1 = \mu_2 = 0.2$, G = 7 × 10^6 Pa, and $R_1 = R_2 = 0.0012$ m into Equations (10)–(12), the normal stiffness coefficient $r_n = 9 \times 10^6$ N/m and tangential stiffness coefficient $r_s = 4.5 \times 10^6$ N/m could be solved.

Through considerable studies on the "Hertz–Mindlin with Bonding" model, existing research [31] has suggested that the critical normal and tangential stresses between particles had a minor effect (<2%) on the elastic modulus and Poisson's ratio of particle bonding model. The elastic modulus and Poisson's ratio of the particle agglomerate model characterize the mechanical properties of the agglomerate when the agglomerate collides with the sieve surface, such that the critical normal and tangential stresses have less effect on the simulation experiments. In accordance with the relevant literature on bonded materials [32,33], the bonding parameters of the frass agglomerate are set (Table 2).

Table 2. Bond parameters of frass particles.

Parameters	Value
Normal stiffness coefficient/(N·m^{-1})	9×10^6
Shear stiffness coefficient/(N·m^{-1})	4.5×10^6
Normal critical stress/Pa	50,000
Shear critical stress/Pa	20,000

2.3.3. Discrete Element Modeling of Black Soldier Fly Larvae

Since the material of the sieve surface is steel, its stiffness is significantly greater than that of the frass aggregates and BSFL, such that the dynamic effect of the frass aggregates on the BSFL can be ignored. The variation of BSFL in body length is dependent on their biological characteristics, presenting both straight and curled forms, to simulate the movement characteristics of BSFL in different postures on the sieve surface with different parameters. Thus, in this experiment combined with the actual separation conditions, the discrete element method was adopted to establish the simulation model of BSFL into two types (including straightening and curling), which was made of multi-spherical particles. The BSFL was 0.023 m in length if it was straight, 0.019 m in length if it was curled, and 0.0049 m in width if it was in either form, as shown in Figure 6. The number of BSFL in the straight and curled states was distributed at 3:2, and a total of 90 straight BSFL and 60 curled BSFL were generated for this simulation experiment. The intrinsic and contact parameters of BSFL were adopted from the discrete element model parameters calibrated in the literature [24].

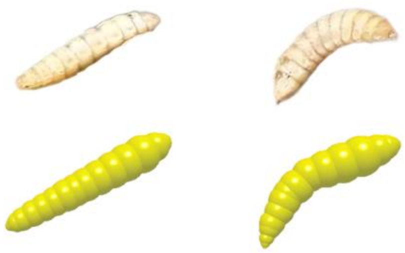

(**a**) (**b**)

Figure 6. Simulation model of black soldier fly larvae. (**a**) Straight BSFL. (**b**) Curled BSFL.

Since the surface mucilage of BSFL in high water content material is relatively high and the surface adhesion is difficult to measure, the contact model is "Hertz–Mindlin with JKR", and the surface adhesion was expressed as surface energy. The total simulation time was set to 5 s, the time step was set to 10% of Rayleigh time step, and the cell size was set to 3 times the minimum particle radius. The compression experiments on BSFL in the literature [34] suggested that after applying a force of more than 3 N to the surface of the polypide, it will cause damage to the extrusion of the polypide of BSFL, such that the critical damage threshold for BSFL was set to 3 N. In other words, when the limit force on the surface of the polypide exceeded the critical damage threshold, the polypide was judged to be damaged.

2.3.4. Geometric Modeling of the Vibrating Screen

The design of the BSF sand sorting device should consider the effect of loose particles of frass with chaotic movements on the sieve surface on the separation effect. However, due to the few fine particles of frass on the curved sieve surface, the effect of loose particles of frass on the fragmentation of frass aggregates and the movement of frass was ignored, and the effect of air resistance was ignored in the process of material throwing off-returning to the sieve surface, so as to simplify the simulation process. The linear vibrating screen was set as a reference object for 3D modeling, with the screen body inlet height of 0.4 m, the sieve surface length of 0.7 m, and the screen body height of 0.2 m. The reason for this is that the particle cluster in the sieve surface lateral distribution is more uniform in the vibrating screen work. Thus, to save the amount of calculation, the sieve surface width was set to 0.15 m, the sieve hole type was selected as square, and the simulation model is illustrated in Figure 7.

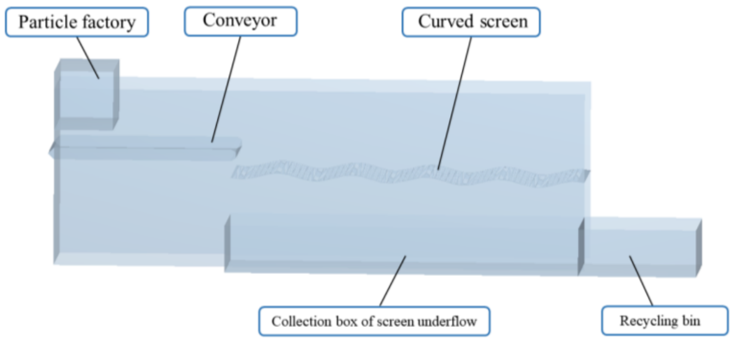

Figure 7. Discrete element model of vibrating screen.

Combined with different sieve surface combination vibration separating operation process and characteristics, the focus was placed on the curved screen as the object of study in the front of the surface screen to build a conveyor model. The model conveying speed is equal to the actual BSF sand on the plane screen movement speed of 0.2 m/s. To simulate the jumping of agglomerates and polypides when moving from the front sieve surface to the back, the conveyor height was elevated by 0.02 m compared with the curved sieve surface, and a particle factory was set at the front of the conveyor belt to generate all the agglomerates in 0.2 s. The particle replacement was completed in 0.3 s, and the diameter of small particles in the agglomerates was set to 0.0025 m. The simulation time was set to 5 s for sufficient fragmentation and separation of frass aggregates, the time step was taken as 10 % of Rayleigh time step, and the cell size was 3 times the minimum particle radius. The generated agglomerates moved with the conveyor to the inlet and were crushed under the action of the vibrating screen for the separation operation.

2.4. Analysis of the Movement of the BSF Sand Mixture on the Curved Screen

The BSF sand mixture is thrown off the sieve surface under the action of the vibrating sieve surface in the trough–crest rise section, and its initial velocity when it is thrown up is equal to the linear velocity of the movement of the BSF sand mixture along the valley–peak rise section, and for the sake of simplifying the analysis, the effect of the uneven force between the particles due to the fragmentation and dispersion of the frass aggregates is ignored. The BSF sand mixture moves uniformly in a horizontal direction; in a vertical direction, the BSF sand mixture first decelerates uniformly with acceleration down and velocity up; after reaching the highest point of throwing off, the BSF sand mixture accelerates uniformly with direction down; Figure 8 depicts the motion trajectory of the BSF sand mixture after it is thrown off by the sieve surface.

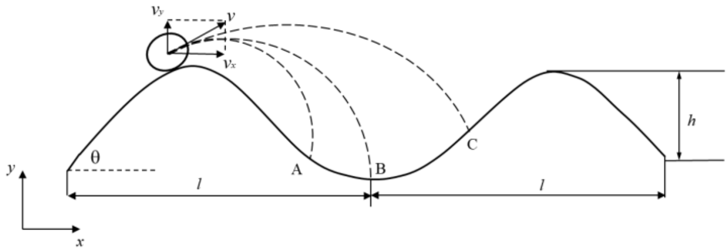

Figure 8. Throwing trajectory of BSF sand mixture on curved screen.

There are several possible contact points for the BSF sand mixture to fall back to the sieve surface:

1. Smooth sliding occurs in the descending section of the crest–trough of the curved sieve surface, namely, point A in Figure 8;
2. Translational tumbling is generated at the trough of the curved sieve surface, namely, point B in Figure 8;
3. The trough–crest rising section of the next curved element generates a bouncing backflow, namely, point C in Figure 8.

When the throwing distance is too small, the BSF sand separation effect is unsatisfactory, and the greater collision effect may hurt the larvae when the throwing distance is too large. Consequently, the motion of the BSF sand mixture on the sieve surface was analyzed, and its horizontal and vertical velocities of being thrown up at the crest of the wave were as follows:

$$v_x = vcos\theta \tag{13}$$

$$v_y = vsin\theta - gt \tag{14}$$

where v_x denotes the horizontal velocity of the BSF sand mixture, in m/s; v_y represents the vertical velocity of the BSF sand mixture, in m/s; θ is the inclination angle of the curved screen unit (°); t expresses the time when the BSF sand mixture is thrown away in the air, in s.

After the BSF sand was thrown up by the sieve surface, its displacement in the horizontal and vertical directions are written as:

$$x = vtcos\theta \tag{15}$$

$$y = vtsin\theta - \frac{1}{2}gt^2 \tag{16}$$

Being thrown up, the maximum height h_0 reached by the BSF sand in the vertical direction is:

$$h_0 = \frac{v^2\sin^2\theta}{2g} \tag{17}$$

BSF sand was thrown away, back to the position of the sieve surface affecting its collision effect and incidence angle. When the BSF sand was thrown to the highest point, under the action of gravity, the vertical direction began to proceed downward in a uniformly accelerated motion, the total fall height of $h_0 + h$. To the highest point, the time t_0 spent by the BSF sand is expressed as:

$$t_0 = \frac{vsin\theta}{g} \tag{18}$$

Accordingly, in the height range of h_0, the movement time of BSF sand is $2t$, and its total throwing distance is written as:

$$L = \frac{v^2\sin^2\theta}{g} \tag{19}$$

Moreover, the speed of the linear vibrating screen is determined by the following equation:

$$\begin{cases} v = \vec{v_x} + \vec{v_y} \\ \vec{v_x} = -\omega r sin\omega t \cdot \cos(\alpha + \beta) \\ \vec{v_y} = -\omega r sin\omega t \cdot \sin(\alpha + \beta) \end{cases} \tag{20}$$

where r denotes the amplitude, in m; ω is the vibration circle frequency, in rad/s; t is the time, in s; α is the vibration direction angle (°); β is the sieve surface inclination (°).

The above analysis reveals that the main factors for the motion characteristics of BSF sand on the vibrating sieve surface are: amplitude, frequency, curved height, curved width, vibration direction angle, and sieve surface inclination. Besides the factors mentioned previously, the literature [35] has noted that the aperture of the sieve hole significantly affects the permeability of the particles, such that the upper seven factors were selected for the subsequent parameter optimization experiments. The test parameter codes are listed in Table 3.

Table 3. Test parameter code.

Parameter	Value	
	−1	**1**
Amplitude X_1/m	0.01	0.014
Frequency X_2/Hz	7	9
Curved height X_3/m	0.004	0.008
Curved width X_4/m	0.03	0.04
Directional Angle X_5/°	45	55
Inclination X_6/°	0	2
Aperture X_7/m	0.003	0.005

2.5. Test Materials and Equipment

The test materials were obtained from the black soldier fly research base of Hunan Agricultural University. After biotransformation of 4-day-old black soldier fly larvae in kitchen waste with a moisture content of 70% for 12–15 days, the BSF sand mixture collected from the breeding tray was stirred evenly and 2 kg was selected randomly from it. The water content of the black soldier fly sand mixture was measured at 40.2% in an electric blast drying oven, and the frass particles, frass aggregates, and black soldier fly larvae were sorted and weighed. The average mass fraction of each component in the black soldier fly sand mixture was 74.1%, 16.3%, and 9.6%, respectively. As depicted in Figure 9, the test equipment and instruments include the linear vibrating screen, electronic scale, second chronograph, computer, and high-speed camera. The total length of the sieve surface is 1.5 m. According to the preliminary test, most of the fine particles of frass can be screened after a screening distance of 0.8 m. Hence, the length of the planar sieve surface is set as 0.8 m, and the length of the curved sieve surface is set as 0.7 m.

2.6. Test Method and Evaluation Indexes

Based on analyzing the process of throwing and separating BSF sand particles, a discrete element simulation model of BSF sand mixture and sieve surface was established to investigate the influence law of each influencing factor on the crushing of frass aggregates and the damage of polypide. Hence, in this study, we take the rate of impurity and injury rate as evaluation indexes, perform simulation experiments to research the better parameter combinations, to verify the correctness of the optimization results through actual tests. The evaluation indexes are calculated as follows:

$$Y_1 = \frac{k_1}{k_0} \times 100\% \tag{21}$$

where Y_1 is the impurity content in the larvae, (%); k_1 represents the mass of the frass in the material at the discharge port of the screen, in kg; k_0 expresses the total mass of the sand mixture at the discharge port of the screen, in kg.

$$Y_2 = \frac{k_2}{k_3} \times 100\% \tag{22}$$

where Y_2 denotes the injury content in the larvae, (%); k_2 represents the number of damaged black soldier fly; k_3 expresses the total number of black soldier fly.

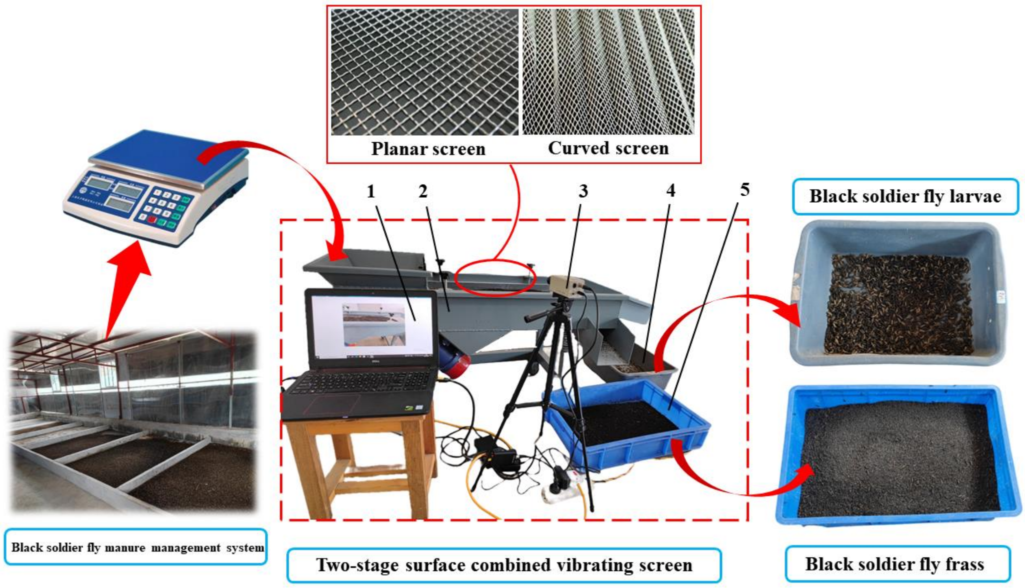

Figure 9. Platform for sorting test of black soldier fly sand mixture. 1. Computer; 2. Vibrating Screen; 3. High-speed camera; 4. Recycling bin at the end of the screen; 5. Collection box of screen underflow.

3. Results

3.1. Factorial Experiment

The Plackett–Burman experiment can significantly decrease the number of trials by comparing the variability of multiple factors at two levels to determine the significant differences between the factors and screen out the key factors from considerable factors, which takes on a great statistical significance. The Plackett–Burman experiment was adopted to further investigate seven factors through the theoretical analysis. The above factors comprised amplitude, frequency, curved height, curved width, vibration direction angle, sieve surface inclination, and aperture. The respective factor was taken as high- or low-level, for a total of 12 sets of tests. In this study, the screening rate Y_3 was introduced to evaluate the fragmentation and separation effect of frass aggregates, i.e., the higher the screening rate, the better the fragmentation and separation effect of aggregates will be.

$$Y_3 = \frac{k_4}{k_5} \times 100\% \tag{23}$$

where k_4 denotes the mass of the agglomerate when it is not sieved, in kg; k_5 represents the mass of the screen underflow, in kg.

The testing program and results are listed in Table 4, and the ANOVA of the test results is listed in Table 5.

As depicted in Table 5, the p-value of the prediction model was lower than 0.05, thus suggesting that the model had a significant effect; the coefficient of determination R^2 was 0.9322, which was close to 1, thus suggesting that the model can account for 93.22% of the test response values; the p-values of the test factors amplitude (X_1) and surface height (X_3) were lower than 0.01, thus suggesting that the two factors significantly affect the vibration separation effect of frass aggregates; the *p*-values of the remaining factors values of the other factors were higher than 0.05, thus suggesting that the other factors do not significantly affect the deconcentration and separation of frass agglomerates. Accordingly, the amplitude, the curved width, the directional angle, the inclination angle, and the aperture diameter were set to 8 Hz, 0.035 m, 50°, 1°, and 0.004 m, respectively. Factors X_1 and X_3 were employed for further simulation tests to study the specific effects of the two critical factors on the response values.

Table 4. Plackett–Burman experiment protocol and results.

No.	X_1/m	X_2/Hz	X_3/m	X_4/m	X_5/°	X_6/°	X_7/m	Y_3/%
1	1	1	−1	1	1	1	−1	65.1
2	−1	1	1	−1	1	1	1	85.2
3	1	−1	1	1	−1	1	1	73.7
4	−1	1	−1	1	1	−1	1	70.4
5	−1	−1	1	−1	1	1	−1	81.5
6	−1	−1	−1	1	−1	1	1	79.4
7	1	−1	−1	−1	1	−1	1	63.8
8	1	1	−1	−1	−1	1	−1	69.3
9	1	1	1	−1	−1	−1	1	75.2
10	−1	1	1	1	−1	−1	−1	78.4
11	1	−1	1	1	1	−1	−1	72.4
12	−1	−1	−1	−1	−1	−1	−1	71.4

Table 5. ANOVA of the Plackett–Burman experiment.

Source of Variance	Sum of Squares	Df	Mean Square	*F* Value	*p* Value	Significance
Model	427.84	7	61.12	7.86	0.0323	*
X_1	182.52	1	182.52	23.47	0.0084	**
X_2	0.16	1	0.16	0.021	0.8918	
X_3	184.08	1	184.08	23.67	0.0083	**
X_4	4.08	1	4.08	0.52	0.5088	
X_5	6.75	1	6.75	0.87	0.4043	
X_6	42.56	1	42.56	5.47	0.0794	
X_7	7.68	1	7.68	0.99	0.3766	
Residual	31.11	4	7.78		R^2	0.9322

Note: ** means very significant ($p < 0.01$); * means significant ($0.01 < p < 0.05$).

3.2. The Effect of the Curved Height on the Fragmentation and Separation of Frass Aggregates

The curved height of the sieve surface directly affects the number of tumbling times and throwing height of the frass agglomerates on the sieve surface. Moreover, under the effect of the vibration excitation of the sieve surface, the frass agglomerates thrown obliquely fell onto the sieve surface, thus promoting them to be broken and separated. Given the effect of the curved height on the fragmentation and separation of particle agglomerates, 0.004 m, 0.005 m, 0.006 m, 0.007 m, and 0.008 m were set as five experimental parameters at 0.001 m intervals, and the results of the fragmentation and separation of frass agglomerates under different curved height conditions were obtained (Table 6).

Table 6. The motion attitude of agglomerates during the separation of different curved heights.

Curved Height	Simulation Time				
	1.8 s	**2.0 s**	**2.2 s**	**2.4 s**	**2.6 s**
0.004 m	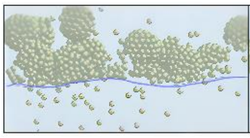	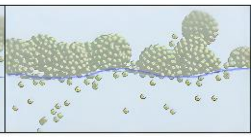	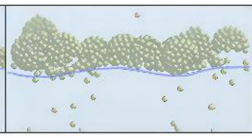	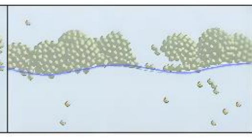	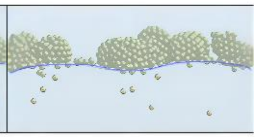
0.005 m	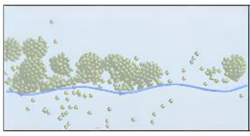	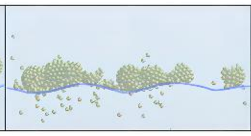	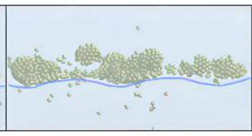	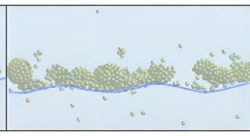	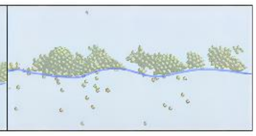
0.006 m	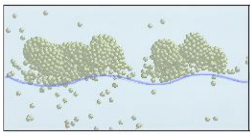	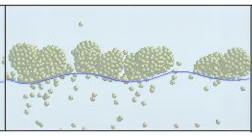	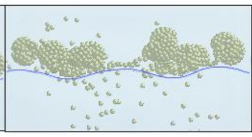	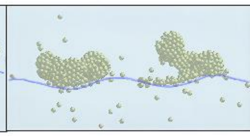	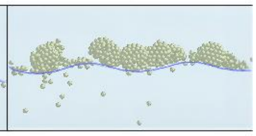
0.007 m	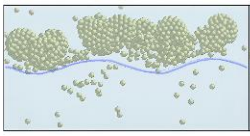	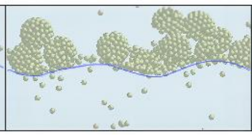	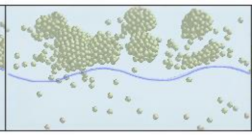	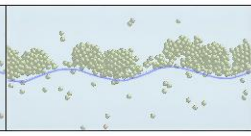	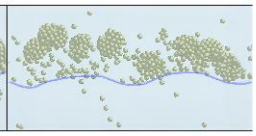
0.008 m	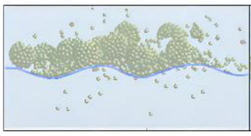	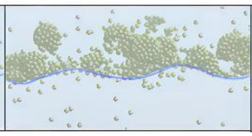	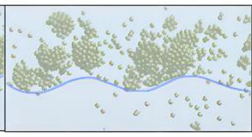	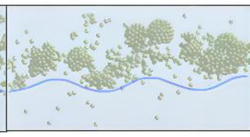	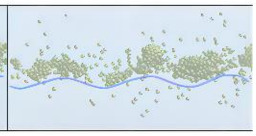

As depicted in Table 6, at the surface height of 0.004 m, the frass agglomerates were almost always close to the sieve surface during the whole transport separation, and only a small amount of fine particles penetrated the screen at the back of the sieve surface. The reason for this result is that after repeated tumbling of the frass agglomerates, the bonding effect of the fine particles at the periphery of the agglomerates tended to decrease, and some of the particles penetrated the screen under the effect of excitation of the drive motor. Thus, the overall non-smooth degree of the sieve surface was low when the height of the curved surface was small, which is consistent with the conventional inclined flat conveying BSF sand separation method and cannot achieve better agglomerate tumbling and crushing ability; these things considered, the separation advantages of the curved sieve surface were not fully used. At the curved surface height of 0.005 m, although the agglomerates remained not thrown away from the sieve surface macroscopically, some of the agglomerates showed a weak rolling–throwing coupling phenomenon. The internal bonding of the agglomerates to the peripheral particles tended to be weakened in the process of movement, and then the agglomerates deformed. Under the action of vibration and shear, some of the frass agglomerates disaggregated through the sieve, and the particles through the sieve were increased compared with 0.004 m, whereas considerable agglomerates remained not disaggregated. In the actual separation operation, the cleaning rate of the worm in the tail collection box will be affected if more agglomerates remain at the end of the screen. With the increase of the surface height to 0.006 m, the movement of frass agglomerates to the crest of the surface generated a slight throwing jump; when they were thrown off and fell back to the sieve surface, the effect of the sieve surface on the agglomerates supplemented the crushing moment applied to the agglomerates. In addition, with the increase in the surface height, the crushing kinetic energy provided by the sieve surface was enhanced, and the degree of agglomeration was further increased, and the number of loose particles through the screen was increased. With the surface height increased to 0.007 m, a significant phenomenon of jumping away from the frass agglomerates on the sieve surface was identified, though the rising section of the wave valley still had a certain supporting effect on the agglomerates. When the agglomerates were thrown from the wave crest to trough, the overall supporting effect of the falling section of the wave trough on the agglomerates was reduced. Moreover, since the sieve surface stiffness was greater, and the effective contact area was smaller, the frass agglomerates were more significantly broken, and the collision separation of considerable secondary agglomerates continued under the combined effect of shear stress and collision effect. The holistic crushing and separation of frass aggregates was more effective at the curved height of 0.007 m. When the surface height was set to the maximum value of 0.008 m, the rising section of the trough–crest and the falling section of the crest–trough were steeper, and the overall non-smoothness of the sieve surface was higher. On that basis, the frass agglomerates generated farther throwing and higher jumping in the process of movement; the normal stress and kinetic energy of crushing applied to the frass agglomerates were increased, and considerable particles were broken away from the bonding constraint and attempted to penetrate the sieve. The crushing pattern was converted from peripheral shedding and local diffusion to complete crushing, and the overall crushing and separation effect was further enhanced.

3.3. Effect of Amplitude on the Fragmentation and Separation of Frass Aggregates

The amplitude significantly affected the crushing and separation effect of frass agglomerates, and the shearing effect on the agglomerates at the trough and the throwing intensity at the crest were increased to a certain extent with the increase in the amplitude, under the condition that other factors remain unchanged. Different particle colors were used to characterize the different velocities of the particles, with red representing larger particle velocities, green indicating medium particle velocities, and blue implying smaller particle velocities. The impact crushing states of the agglomerates under each amplitude condition are shown in Figures 10–14, respectively. As depicted in Figures 10 and 11, when the amplitude of the vibrating screen was 0.01 and 0.011 m, only part of the particle cluster was slightly thrown away from the sieve surface, the overall particle speed was small, and only parts of the particles were separated from the aggregate under the action of friction shear of the sieve surface. The degree of deformation of the frass aggregate was small, and this amplitude was suitable for the crushing and separation of the low-moisture-content frass aggregate. As the amplitude increased to 0.012 m, the height and distance of the agglomerates being thrown up were increased, so that the collision effect of the agglomerates falling back on the sieve surface increased, and the number of red agglomerates increased significantly, namely, the overall velocity of the particles was faster. When the amplitude increased to 0.013 and 0.014 m, the amplitude of the sieve surface movement further increased, the collision between the frass aggregates and the sieve surface is more intense, and the aggregates had greater crushing kinetic energy. The internal bonding torque of the particle aggregates was less than the crushing torque applied to the particles from the outside, and could not continue to restrain the detachment of the external particles, so the frass particles gradually changed from the state of clusters to the discrete state. Considerable fine particles get the opportunity to penetrate the screen, and have a better crushing and separating effect.

As depicted in Figures 10–14, the overall velocity of the frass agglomerates was higher when the agglomerates were being thrown off the falling section of the wave crest–trough. Moreover, once they reached the wave trough, they were promoted to climb with the increasing section of the wave trough–crest, and the velocity was slower at this point. Afterward, if they reached the wave crest, they were thrown back to the wave trough by the sieve surface, the velocity increased again, and so forth; the overall velocity of frass aggregates exhibited an alternating pattern of “fast–slow–fast–slow”.

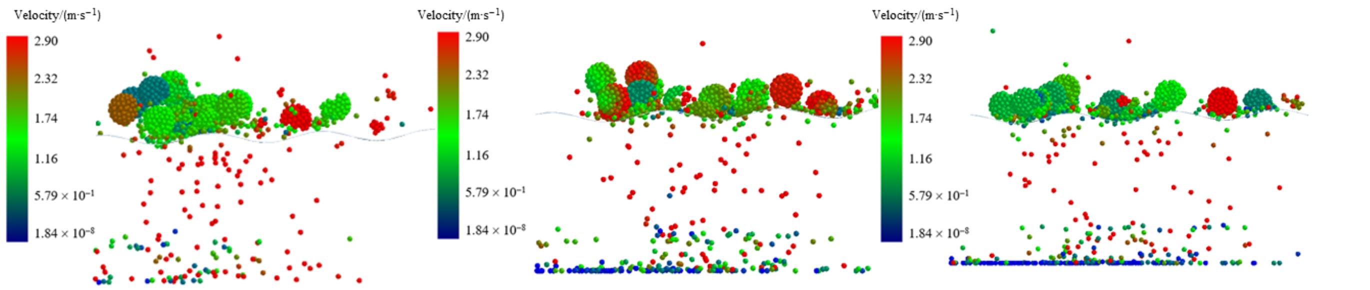

(**a**) (**b**) (**c**)

Figure 10. Velocity graph of frass agglomerates at an amplitude of 0.01 m. (**a**) t = 1.8 s. (**b**) t = 2.2 s. (**c**) t = 2.6 s.

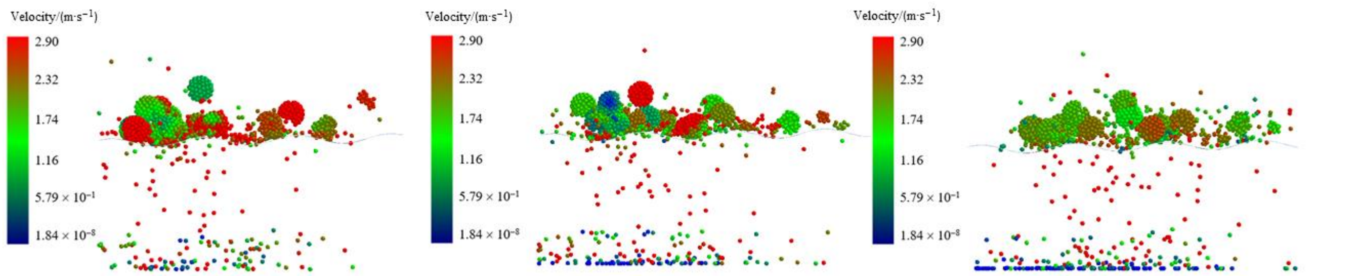

(**a**) (**b**) (**c**)

Figure 11. Velocity graph of frass agglomerates at an amplitude of 0.011 m. (**a**) t = 1.8 s. (**b**) t = 2.2 s. (**c**) t = 2.6 s.

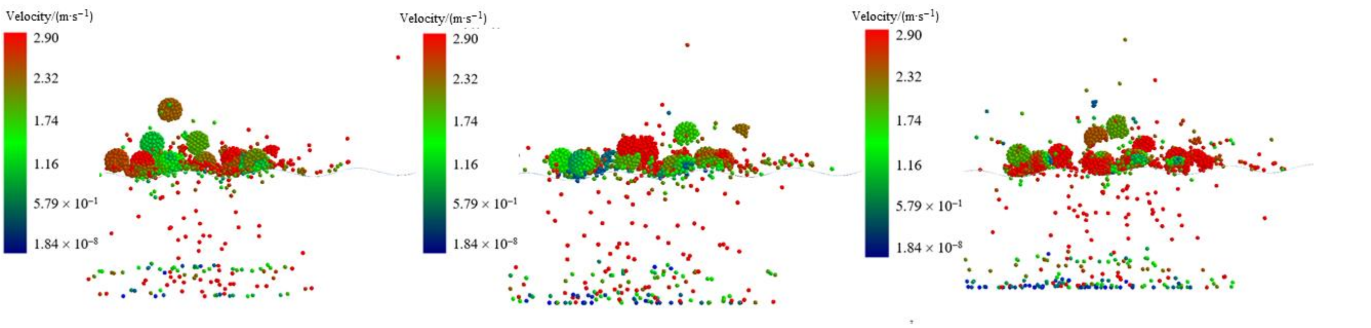

(**a**) (**b**) (**c**)

Figure 12. Velocity graph of frass agglomerates at an amplitude of 0.012 m. (**a**) t = 1.8 s. (**b**) t = 2.2 s. (**c**) t = 2.6 s.

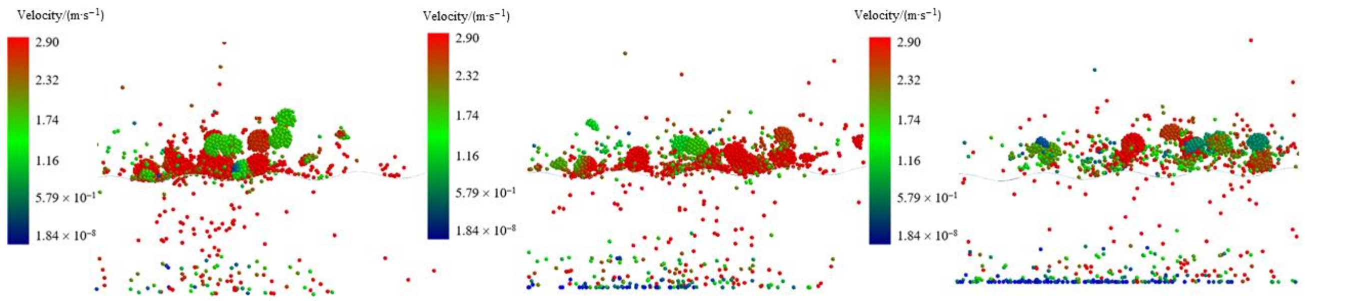

(**a**) (**b**) (**c**)

Figure 13. Velocity graph of frass agglomerates at an amplitude of 0.013 m. (**a**) t = 1.8 s. (**b**) t = 2.2 s. (**c**) t = 2.6 s.

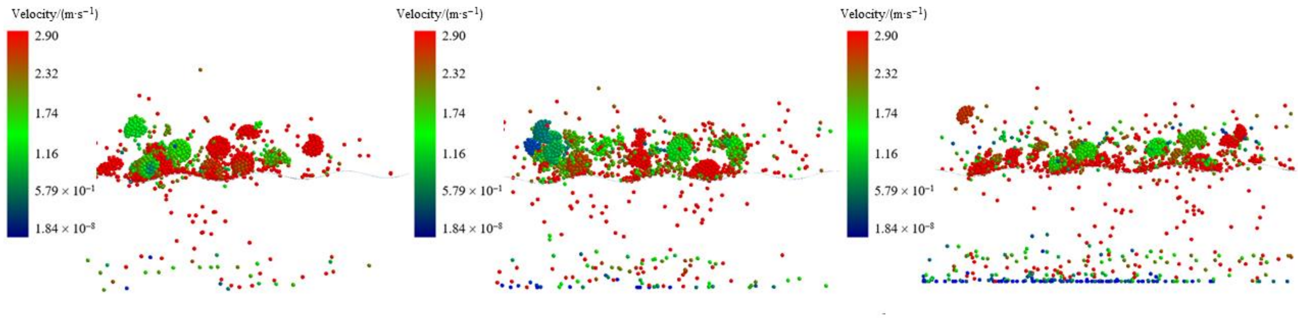

Figure 14. Velocity graph of frass agglomerates at an amplitude of 0.014 m. (**a**) t = 1.8 s. (**b**) t = 2.2 s. (**c**) t = 2.6 s.

3.4. Effect of Amplitude and Curved Height on the Collision Characteristics of the Black Soldier Fly Larvae

The main operation purpose of the back section surface screen refers to the vibrational separation of frass agglomerates, and the main factors for the vibrational separation of agglomerates include amplitude and curved height. Thus, the collision characteristics of BSFL under the effect of different curved heights and amplitudes were studied (Figure 15). As depicted in the figure, with the increase in the curved height and amplitude, the pressure on the bodies of the BSFL tended to increase; at the amplitude of 0.014 m and the curved height of 0.006, 0.007 and 0.008 m, respectively, the ultimate pressure on the polypide exceeded its critical damage threshold. The extrusion damage to the BSFL increased, and the separation quality was not ensured. Moreover, the smaller amplitude and surface height had less effect on the BSFL, whereas they made the sieve surface drive the BSF sand mixture with a slight throwing effect, similar to the separation method of inclined flat conveying. The particle backflow phenomenon was significant, and the separation effect was poor, such that the appropriate amplitude and curved height should be selected for the vibration separation of the BSFL sand mixture. As a result, subsequent tests were performed by selecting the amplitudes of 0.011, 0.012 and 0.013 m and the curved heights of 0.005, 0.006 and 0.007 m, respectively, to collect the pressure on the BSFL under the above parameters to examine the damage prevention effect of the BSFL on the curved sieve surface.

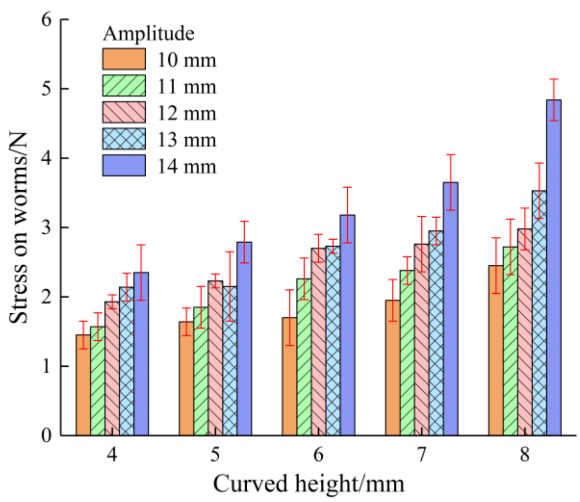

Figure 15. Ultimate pressure on black soldier fly larvae at different amplitudes and curved heights.

Figure 16 presents the average force variation curves of the BSFL particles population at different amplitudes and curved heights. As depicted in Figure 16a, the two peaks of the pressure applied by the sieve surface on the straight BSFL body surface reached

1.97 N and 1.66 N at an amplitude of 0.011 m and a curved height of 0.005 m, respectively. The two pressure peaks on the curled BSFL surface reached 0.37 N and 0.33 N, i.e., the pressure on the straight BSFL was significantly greater than that on the curled BSFL. The possible reason for the above result is that the straight BSFL had some tumbling back and collision effect on the sieve surface. As depicted in Figure 16b, with the amplitude kept constant and the curved height increased to 0.006 m, the two pressure peaks of the straight BSFL reached 2.54 N and 0.3 N, respectively, while those of the curled BSFL were 0.2 N and 0.09 N, respectively. The pressure on the straight BSFL was also significantly greater than that on the curled BSFL. The force patterns of the two states with the curved height increased to 0.007 m are presented in Figure 16c, in which the two pressure peaks reached 1.69 N and 1.58 N for the straight BSFL, 2.4 N and 1.1 N for the curled BSFL, respectively. With the increase of the curved height to 0.007 m, the maximum pressure on the curled bodies was greater than that on the straight ones, whereas the pressure on the straight ones had several peaks and remained high. As depicted in Figure 16a–c, when the amplitude was kept constant at the level of 0.011 m, the peak pressure of the BSFL under both states changed with the increase in the curved height, and the overall trend was increasing.

As depicted in Figure 16d, at the amplitude of 0.012 m and the curved height of 0.005 m, the two peak pressures on the straight and curled BSFL reached 2.12 N and 0.92 N, as well as 1.36 N and 0.36 N, respectively; the pressure on the straight was greater than that on the curled BSFL. Likewise, the peak impact force was greater than that of the curled BSFL since it was easier to roll on the sieve surface. As depicted in Figure 16e, with the increase of the surface height to 0.006 m, the two pressure peaks of 2.6 N and 0.91 N were applied to the straight BSFL, and the pressure peaks of 0.26 N and 0.21 N were applied to the curled BSFL, probably due to the poor mobility of the curled BSFL. With the increase in the height of the curved surface, the ability of the curved sieve surface to drive the curled BSFL strengthened, and the tumbling back phenomenon of the curled BSFL was reduced. As a result, the collision effect with the sieve surface was lighter. As depicted in Figure 16f, when the amplitude was kept constant at 0.012 m and the surface height was increased from 0.006 m to 0.007 m, the two pressure peaks for the straight BSFL reached 1.5 N and 1.23 N, respectively, while the two pressure peaks for the curled BSFL reached 2.68 N and 0.9 N, respectively. Similar to Figure 16c, the maximum pressure on the curled BSFL was greater than that on the straight BSFL, whereas the overall pressure peaks for the straight BSFL were kept at a higher level. The possible reason for the above result is that at this parameter level, the curled BSFL was attached to the curved sieve surface; at the higher height of the curved, the attached BSFL was thrown from the crest to the trough. Furthermore, the momentum theorem suggests that the higher the throwing height of the BSFL, the greater the instantaneous impact at the trough will be, such that the pressure on the curled BSFL was higher at this time.

As depicted in Figure 16g, at the amplitude of 0.013 m and the curved height of 0.005 m, the two pressure peaks of the sieve surface reached 1.77 N and 1.48 N for the straight BSFL, 2.41 N and 1.03 N for the curled BSFL, which were more stable for the straight BSFL and more scattered for the curled BSFL. The reason for the above results is the tumbling of individual straight insects on the sieve surface, thus resulting in obstructed transport and multiple collisions with the sieve surface; moreover, the poor tumbling performance of the curled BSFL primarily explained why the maximum pressure of curled insects was greater than that of the straight BSFL. As depicted in Figure 16h, when the curved height increased to 0.006 m, the two pressure peaks of the straight BSFL reached 0.75 N and 0.51 N, respectively, and the two pressure peaks of the curled BSFL were 3.05 N and 2.42 N, respectively. The higher pressure was identified during the collision process when the BSFL was thrown down to the trough twice, thus suggesting that the phenomenon of the material thrown up by the curved sieve surface became more and more significant with the increase in the amplitude and curved height. Furthermore, the peak pressure of the curled BSFL exceeded the critical damage threshold, thus suggesting that the BSFL was easy to lose protection and cause damage (e.g., tangential abrasion) when colliding on the sieve surface of this parameter combination. After the curved height increased to 0.007 m, as presented in Figure 16i, the two maximum pressures on the straight BSFL reached 3.75 N and 1.12 N, respectively, and the two maximum pressures on the curled BSFL were examined as 1.33 N and 0.73 N, respectively. The maximum pressures on the straight BSFL exceeded the critical damage threshold and became more dispersed. The major reason for the above results is the increased vibration amplitude of the sieve surface and the increased height difference between crest and trough, thus increasing the overall transport speed of the BSFL and causing a stronger effect on the sieve surface; the extension of the stagnation time of individual insects led to the decreased frequency of collision contact and the increased collision intensity, such that the BSFL was extremely prone to the extrusion damage phenomenon.

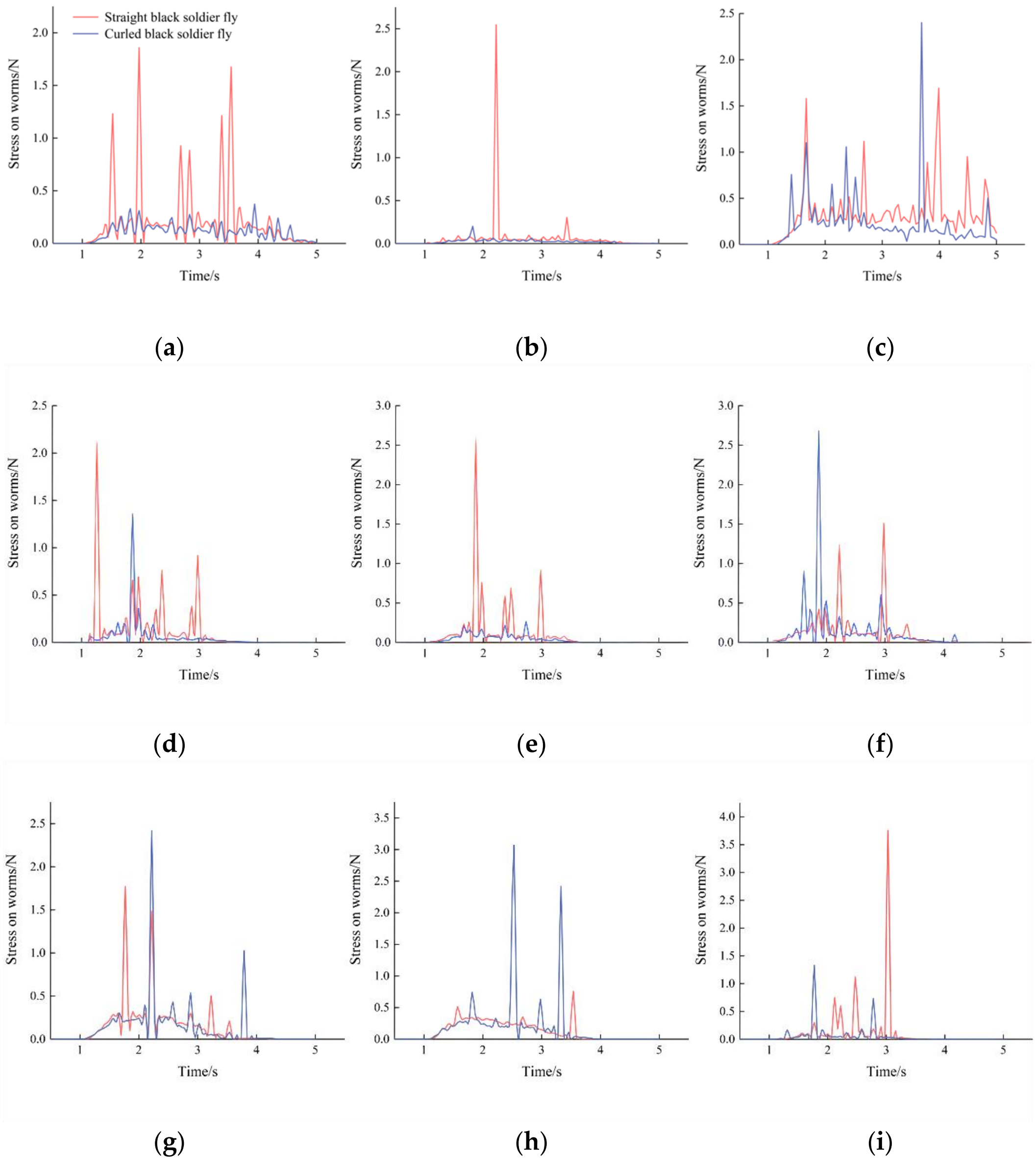

Figure 16. Force analysis in the separation movement of black soldier fly. (**a**) X_1 = 0.011 m, X_3 = 0.005 m. (**b**) X_1 = 0.011 m, X_3 = 0.006 m. (**c**) X_1 = 0.011 m, X_3 = 0.007 m. (**d**) X_1 = 0.012 m, X_3 = 0.005 m. (**e**) X_1 = 0.012 m, X_3 = 0.006 m. (**f**) X_1 = 0.012 m, X_3 = 0.007 m. (**g**) X_1 = 0.013 m, X_3 = 0.005 m. (**h**) X_1 = 0.013 m, X_3 = 0.006 m. (**i**) X_1 = 0.013 m, X_3 = 0.007 m.

Figure 17 presents the resultant velocity magnitude variation curves of BSFL at different amplitudes and curved heights. The combination of force characteristics and absolute velocity magnitude variation of the BSFL can better explain the movement process of BSFL on the sieve surface. Within 0~5 s, the BSFL movement process went through three stages as follows: At the first stage, the BSFL moved forward on the conveyor at a speed of 0.2 m/s, performing a uniform linear motion at this time, and the velocity magnitude remained constant. At the second stage, the BSFL fell into the curved sieve surface under the action of gravity, and the BSFL were driven by the sieve surface in a reciprocal motion of "throwing up—falling back—throwing up", with fluctuating speed. At the third stage, after the BSFL were thrown up at the end of the screen, they fell into the outlet collection box under the action of gravity, and the velocity decreased rapidly, which fluctuated in a smaller range when coming into contact with the box and produced some collision rebound, but the duration was short and finally tended to be constant, namely, the separation–harvesting link between the BSF organic fertilizer and the BSFL was completed.

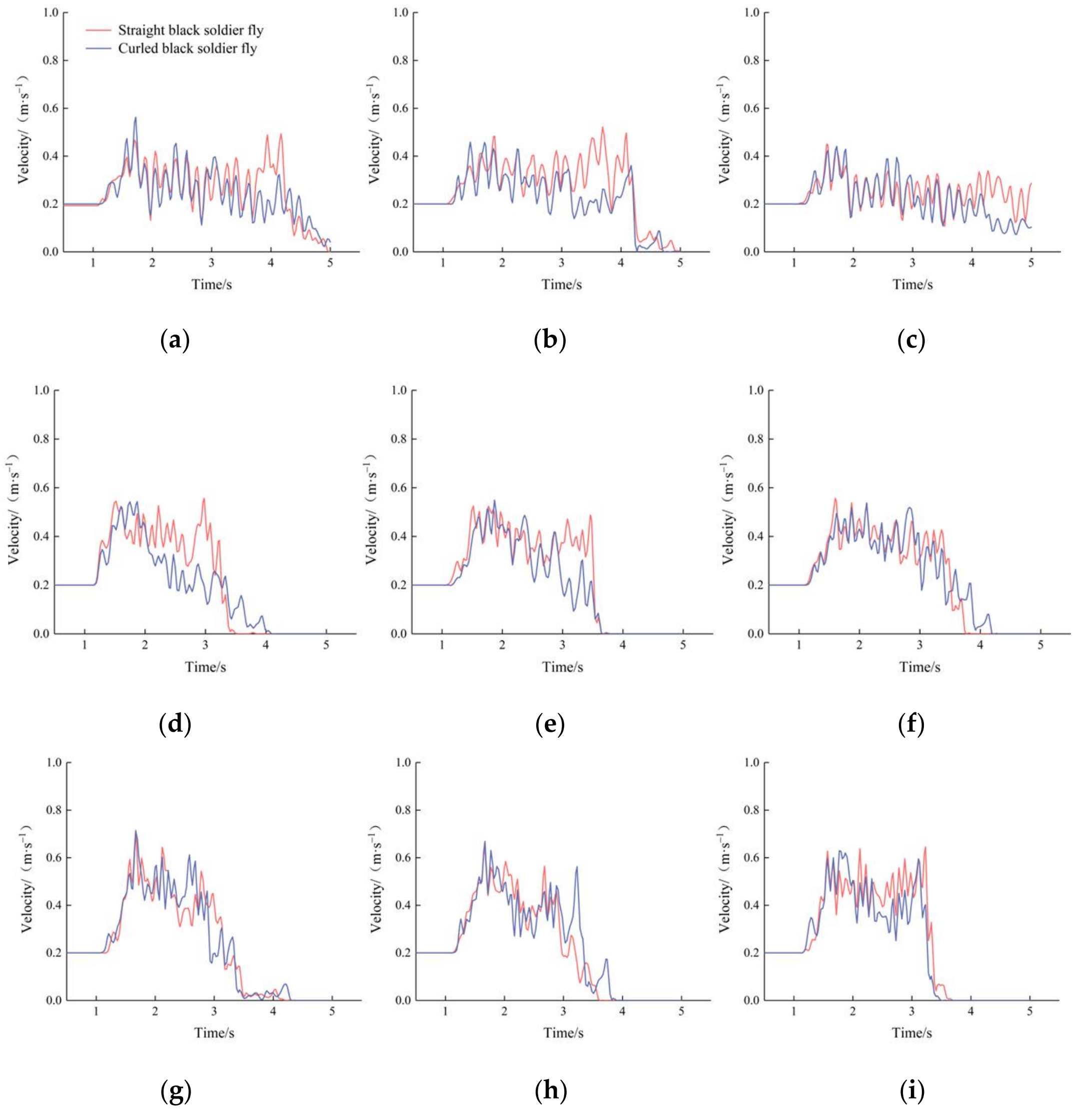

Figure 17. Resultant velocity magnitude analysis in the separation movement of black soldier fly. (**a**) X_1 = 0.011 m, X_3 = 0.005 m. (**b**) X_1 = 0.011 m, X_3 = 0.006 m. (**c**) X_1 = 0.011 m, X_3 = 0.007 m. (**d**) X_1 = 0.012 m, X_3 = 0.005 m. (**e**) X_1 = 0.012 m, X_3 = 0.006 m. (**f**) X_1 = 0.012 m, X_3 = 0.007 m. (**g**) X_1 = 0.013 m, X_3 = 0.005 m. (**h**) X_1 = 0.013 m, X_3 = 0.006 m. (**i**) X_1 = 0.013 m, X_3 = 0.007 m.

The comparison of Figure 17 with the same surface height and different amplitudes, in combination with the mechanical characteristics of Figure 16, indicated that the velocity curves of the two states of the BSFL were distributed in the transverse and longitudinal directions with little difference, thus suggesting that the motion time of the two states of the BSFL on the sieve surface was nearly the same. As depicted in Figure 17a–f, with the increase in the amplitude and surface height, the velocity of BSF sand on the sieve surface tended to increase; at the amplitude of 0.012 m and the curved height of 0.007 m, the velocity of BSFL reached a higher level, and the frass agglomerates on the sieve surface achieved larger crushing kinetic energy, thus increasing the degree of fragmentation and separation. In any case, the peak pressure on BSFL at this time did not exceed the critical threshold value, thus suggesting that the BSFL can achieve a better effect of disaggregation and separation of BSFL agglomerates simultaneously. At the amplitude of 0.013 m and the curved height of 0.005 m, the velocity distribution characteristics and velocity variation law of BSF sand on the sieve surface were more similar to Figure 17f, thus suggesting that the movement of the BSF sand on the surface with two parameters was more comparable and exerted a more significant crushing and separation effect. These things considered, the pressure of BSF on the surface of both screens did not exceed the mechanical range of critical damage of the BSFL. When the amplitude was 0.013 m and the curved height was increased to 0.006 and 0.007 m, the worms moved faster, and the peak pressure from the sieve surface was greater than the critical threshold, thus suggesting that the BSFL will be significantly damaged by the collision and extrusion of the sieve surface. Accordingly, the combination of parameters does not apply to the actual BSFL sand sorting.

In brief, under the same sieve surface separation distance, the amplitude and surface height contributed to the separation effect of frass crushing, thus suggesting that the separation effect of frass on the curved sieve surface was improved with the increase in the amplitude or the curved height, such that a larger surface height or amplitude should be selected as much as possible. The simultaneously increased values of the two parameters will lead to better collisional depolymerization of the agglomerates, but, at the same time, will lead to more serious damage to the BSFL. The better parameter combinations were 0.012 m amplitude, 0.007 m curved height, and 0.013 m amplitude, 0.005 m curved height. The frass agglomerates were basically broken at the end of the surface screen, and the agglomerates were disaggregated into considerable fine particles through the screen, and the frass agglomerates and BSFL were separated.

3.5. Parameter Verification Test

A vibrating separation test was performed in the comprehensive training center of Hunan Agricultural University to verify the screening performance of the two-stage surface combined vibrating screen. The amplitude and curved height were set based on the optimal combination of parameters. The test was performed five times for the respective group, and the results were averaged (Table 7).

Table 7. Results of tests.

No.	Preferred Parameters		Impurity Rate/%	Injury Rate/%
	X_1/m	X_3/m		
1	0.012	0.007	2.34	5.65
2	0.013	0.005	3.15	4.3

In Table 7, the larvae–frass separation of BSF under the better combination of parameters was better, consistent with the simulation test results, and the relative errors were 2.86~10.38% between the actual test and the simulation test. As depicted in Figure 18, there were fewer frass particles at the back of the screen, thus suggesting that the separation of frass and larvae is effective. Similar to the simulation, Both the straight BSFL in the red frame and the curled BSFL in the yellow circle have a "throwing up—falling back—throwing up" movement at the back of the sieve surface. To be able to accurately track the target particles in the particle population, the image from high-speed camera was divided into a grid (Figure 18). The exact coordinates of the target particles were obtained by locating them on the grid at a certain moment. The position coordinates of the target particle were extracted every 0.02 s, and the average velocity obtained from this displacement compared with the interval time served as the instantaneous velocity of the particle. The average horizontal velocities of 20 BSFL in the straight and curled states on the sieve surface in the time period from 3.8 to 5.0 s were extracted, thus suggesting that the changes of horizontal velocities of BSFL in both states on the sieve surface, are consistent with the numerical simulation results. The above result verified the accuracy of the simulation test and the reliability of the optimal parameters, by which the test can further enhance the screening performance of the BSF sand mixture sorting device.

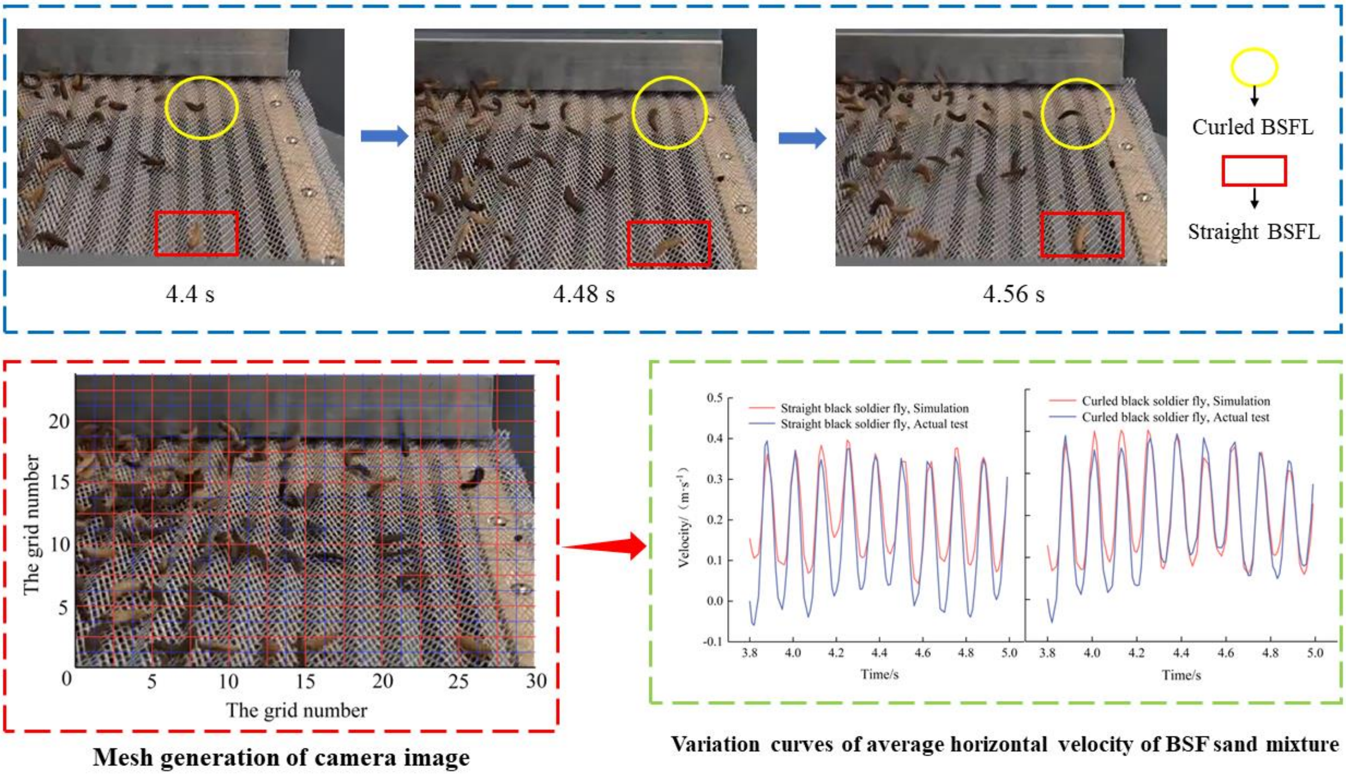

Figure 18. Comparison of actual and simulated images of larvae movement at the screen tail.

4. Discussion

How to separate and harvest BSF to be pupated from considerable BSF sand mixture as soon as possible is one of the key problems to be solved in the development and promotion of BSF culture. BSF frass agglomerates exhibit high quantity, and they are difficult to separate due to the existence of certain water in the pores between the frass particles, the formation of liquid bridges between the particles, the phenomenon of adhesion, and the presence of considerable fine particles agglomerates inside the BSF sand mixture. Given the above characteristics of the agglomerates, a two-stage sieve surface vibration separation device was developed by dividing the sieve surface into two sections and using combined planar and curved screen vibration. Compared with the conventional planar screen, the crest and trough structure of the curved screen is more conducive to multiple collision and tumbling of aggregates, and the internal structure of the agglomerates will be broken and depolymerized by sudden changes. Tao et al. [36] developed a combined sieve surface root–soil separation device for radix isatidis, which achieved better root–soil separation performance by combining a diagrid screen with a sieve plate screen. Wei et al. [37] designed a potato harvester with a multi-stage separation process, which divided the sieve surface into four stages and achieved a high soil crushing rate and a low potato injury rate for harvesting. The comparison of the experimental results of the two-stage sieve surface vibrating separation device with existing research [36,37] suggests that the separation performance can be further enhanced by dividing the sieve surface into multiple segments for the complex composition of the materials to be separated. However, unlike the radix isatidis and potatoes, the polypide of BSF is less rigid and highly susceptible to damage when colliding with the curved screen. Accordingly, the parameter optimization test for selecting the appropriate vibration parameters can avoid the polypide to a certain extent, to separate the damage reduction.

In this study, the effect of the critical parameters of the curved screen on the separation of agglomerates and the force on the BSFL were analyzed based on a model built for agglomerates and BSFL. The process of BSF sand mixture separation was simulated and analyzed using the discrete element method to obtain a better combination of parameters. Under the above combination of parameters, the actual sorting experiments were performed. As revealed by the comparison of the screen images and sieving results between the simulated and actual tests, the simulated tests achieved better accuracy, with the absolute value of the maximum relative error of 10.38%. Similar to the results in the literature [38], it might be caused by the fact that the shapes of the worm bodies in the actual sorting process are diverse, whereas this simulation experiment only set them to two shapes, such that some additional data errors were generated. For the actual sieving application, the above errors are acceptable to a certain extent, and the simulation experiment results can provide some reference for the parameter setting of the sieving device. In general, the simulated predictions are well consistent with the actual test values.

5. Conclusions

(1) For the black soldier fly sand mixture characteristics and separation requirements, based on the earlier design, the key part of the curved sieve surface working parameters of the two-stage sieve surface vibrating separation device was optimized, and for the black soldier fly larvae, the frass small particles, and the frass agglomerates, a fast and clean separation harvest was better achieved.

(2) Based on the model of frass agglomerates and black soldier fly larvae, the sieve surface parameters significantly affecting BSF sand mixture separation were selected through the Plackett–Burman test. The effects of the sieve surface parameters on the fragmentation and separation process of frass agglomerates, together with the collision motion characteristics of worm bodies, were discussed. As the amplitude of the vibrating screen was maintained at 0.011 and 0.012 m through the simulation analysis, with the curved height increasing from 0.005 m to 0.007 m, the peak pressure on the worm body was less than the critical damage threshold, such that the black soldier fly larvae damage reduction control can be achieved in the separation process; at the amplitude of 0.013 m and the curved height of 0.005 m, the peak pressure on the worm body still did not break the critical threshold, whereas when the curved height increased to 0.006 and 0.007 m, the peak pressure on the larvae exceeded the critical damage force, and the larvae was significantly damaged.

(3) The comparison and analysis results of the aggregates crushing test and the black soldier fly collision test suggested that although using larger amplitude and curved height can make the aggregates crush and separate better, it created irreversible damage to the larvae and seriously affected the economic efficiency of the black soldier fly breeding industry. Hence, after comparing the effect of cluster breaking and larvae collision characteristics of a wide variety of simulation tests, the optimal parameter combinations were selected as: 0.012 m amplitude and 0.007 m curved height, when the impurity rate in the collection box was 2.34% and the larvae injury rate was 5.65%; and 0.013 m amplitude and 0.005 m curved height, when the impurity rate and larvae injury rate were 3.15% and 4.3%, respectively. The difference between the simulation test and the physical test was minor, which can conform to the actual operational requirements.

(4) Besides BSF frass, the curved screen is also more effective in vibrating and crushing granular agglomerates (e.g., agricultural soil). Thus, in the crop–soil system, if there

is a low cleaning rate, the installation of the curved screen in the back section of the screen surface can be considered. Furthermore, this study applies to a sinusoidal curved surface screen, and further research should be conducted to determine whether a curved screen with a different curve type can enhance the cleaning performance. The scale and mechanization of black soldier fly breeding are still in their initial stage in China, but the development speed is fast, the research is limited, and the application scope is insufficient. There is still a lot of fundamental work to be further developed and improved in this field in the future. This study only focuses on the material separation technology in the later stage of black soldier fly breeding, with the refinement, automation, and intelligence of black soldier fly breeding; further research can be carried out on the systematic equipment for taking, separating, harvesting, and conveying of material in the later stage of black soldier fly breeding. In the actual application, using the technology principles and parameter optimization methods in this article, we can develop different equipment for separating and harvesting black soldier fly sand mixture in different scales, and for different breeding scenarios, to meet the requirements of integrated and mechanized separation and harvesting of black gadfly in the late stage of breeding.

Author Contributions: Conceptualization, methodology, writing—original draft preparation, writing—review and editing, S.S. (Shisheng Song); software, validation and data curation, Y.W.; formal analysis and investigation, T.Z.; resources and visualization, S.S. (Songlin Sun); supervision and project administration, Y.Y.; supervision, project administration and funding acquisition, C.P. All authors have read and agreed to the published version of the manuscript.

Funding: A Project Supported by Scientific Research Fund of Hunan Provincial Education Department (Grant No. 22A0169).

Institutional Review Board Statement: Not applicable.

Informed Consent Statement: Not applicable.

Data Availability Statement: All data are presented in this article in the form of figures and tables.

Conflicts of Interest: The authors declare no conflict of interest.

References

1. Ji, D.; Yao, Z.S.; Zhang, C.; Wei, Z.H.; Zong, Z.L.; Su, Y.Y. Analysis of microbial community structure in biogas production by anaerobic fermentation of kitchen waste. *Acta Energ. Sol. Sin.* **2022**, *43*, 354–362. (In Chinese)
2. Min, H.H.; Liu, K.L.; Lv, L.Y.; Song, X.X.; Zhang, G.M. Research progress and performance improvement strategies of anaerobic codigestion of food waste. *Chin. J. Environ. Eng.* **2022**, *16*, 2457–2466. (In Chinese)
3. Wang, Y.Y.; Zang, B.; Li, G.X.; Liu, Y. Evaluation the anaerobic hydrolysis acidification stage of kitchen waste by pH regulation. *Waste Manag.* **2016**, *53*, 62–67. [CrossRef] [PubMed]
4. Wang, Y.; Yu, G.H.; Li, Y.Y. Research progress on treatment technology of organic wastes by black soldier fly. *Mod. Agric. Sci. Technol.* **2022**, *10*, 129–135. (In Chinese)
5. Cheng, J.Y.K.; Chiu, S.L.H.; Lo, I.M.C. Effects of moisture content of food waste on residue separation, larval growth and larval survival in black soldier fly bioconversion. *Waste Manag.* **2017**, *67*, 315–323. [CrossRef] [PubMed]
6. Yang, D.M.; Zhu, L.; Zhou, T.J. Research progress of food waste resource treatment technology. *Guangdong Chem. Ind.* **2020**, *47*, 98–99. (In Chinese)
7. Zhang, X.L.; Duan, Y.G.; He, Y.H. Optimization of black soldier fly larvae raising with kitchen waste and chicken manure. *J. Zhejiang Agric. Sci.* **2021**, *62*, 1200–1203+1258. (In Chinese)
8. Diener, S.; Solano, N.M.S.; Gutierrez, F.R.; Zurbrugg, C.; Tockner, K. Biological Treatment of Municipal Organic Waste using Black Soldier Fly Larvae. *Waste Biomass Valorization* **2011**, *2*, 357–363. [CrossRef]
9. Chai, Z.Q.; Wang, F.B.; Guo, M.F.; Wei, Q.H.; Chen, X.F. Research of Stratiomyidae and its utilization. *Guangdong Agric. Sci.* **2012**, *39*, 182–185+195. (In Chinese)
10. Lalander, C.H.; Fidjeland, J.; Diener, S.; Eriksson, S.; Vinneras, B. High waste-to-biomass conversion and efficient *Salmonella* spp. reduction using black soldier fly for waste recycling. *Agron. Sustain. Dev.* **2015**, *35*, 261–271. [CrossRef]
11. Yu, G.H.; Chen, Y.H.; Yu, Z.N.; Cheng, P. Research progression on the larvae and prepupae of black soldier fly *Hermetia illucens* used as animal feedstuff. *Chin. J. Appl. Entomol.* **2009**, *46*, 41–45. (In Chinese)
12. Muller, A.; Wolf, D.; Gutzeit, H.O. The black soldier fly, *Hermetia illucens*—A promising source for sustainable production of proteins, lipids and bioactive substances. *Z. Nat. C* **2017**, *72*, 351–363. [CrossRef] [PubMed]

13. Sthilaire, S.; Sheppard, C.; Tomberlin, J.K.; Irving, S.; Newton, L.; Mcguire, M.A.; Mosley, E.E.; Hardy, R.W.; Sealey, W. Fly prepupae as a feedstuff for rainbow trout, *Oncorhynchus mykiss*. *J. World Aquacult. Soc.* **2007**, *38*, 59–67. [CrossRef]
14. Newton, G.L.; Booram, C.V.; Barker, R.W.; Hale, O.M. Dried *Hermatia illucens* larvae meal as a supplement for swine. *J. Anim.* **1977**, *44*, 395–400.
15. Nguyen, T.; Tomberlin, J.K.; Vanlaerhoven, S. Ability of black soldier fly (diptera: Stratiomyidae) larvae to recycle food waste. *Environ. Entomol.* **2015**, *44*, 406–410. [CrossRef] [PubMed]
16. Xv, F.M.; Wang, G.X.; Huang, X.D.; Huang, Y.H. Large-scale production of black soldier fly (*Hermetia illucens* L.) and its application progress in aquaculture feed. *Chin. J. Anim. Nutr.* **2020**, *32*, 5606–5613. (In Chinese)
17. Dong, K.J.; Yu, A.B. Numerical simulation of the particle flow and sieving behaviour on sieve bend/low head screen combination. *Miner. Eng.* **2012**, *31*, 2–9. [CrossRef]
18. Li, Z.F.; Tong, X. A study of particles penetration in sieving process on a linear vibration screen. *Int. J. Coal Sci. Technol.* **2015**, *4*, 299–305. [CrossRef]
19. Zhou, J.C.; Zhang, L.B.; Hu, C.; Li, Z.H.; Tang, J.J.; Mao, K.M.; Wang, X.Y. Calibration of wet sand and gravel particles based on JKR contact model. *Powder Technol.* **2021**, *397*, 117005. [CrossRef]
20. Ma, Z.; Li, Y.M.; Xu, L.Z. Theoretical analysis of micro-vibration between a high moisture content rape stalk and a non-smooth surface of a reciprocating metal cleaning screen matrix. *Biosyst. Eng.* **2015**, *129*, 258–267. [CrossRef]
21. Fang, Q.; Song, S.S.; Zhou, T.; Peng, C.W.; Sun, S.L.; Zhu, H.Y. Design and experiment of a two-stage segmented drum screening device for black soldier fly insect sand. *J. Agric. Sci. Technol.* **2022**, *24*, 130–139. (In Chinese)
22. Peng, C.W.; Zhou, T.; Song, S.S.; Sun, S.L. Analysis and experiment of feeding material process of *Hermetia illucens* L. frass bucket wheel based on DEM. *Comput. Electron. Agric.* **2022**, *196*, 106855. [CrossRef]
23. Song, S.S.; Sun, S.L.; Fang, Q.; Peng, C.W.; Zhou, T.; Zhu, H.Y. Parameters calibration of discrete element for kitchen waste organic fertilizer bioconversion by black soldier fly. *J. Agric. Sci. Technol.* **2022**, *24*, 123–132. (In Chinese)
24. Peng, C.W.; Zhou, T.; Sun, S.L.; Xie, Y.L.; Wei, Y. Calibration of parameters of black soldier fly in discrete method simulation based on response angle of particle heap. *Acta Agric. Zhejiangensis* **2022**, *34*, 814–823. (In Chinese)
25. Jeroen, D.S.; Enya, W.; Paul, C.; Leen, V.C. Microbial community dynamics during rearing of black soldier fly larvae (*Hermetia illucens*) and impact on exploitation potential. *Appl. Environ. Microbiol.* **2018**, *84*, e02722-17.
26. Jiang, C.L. *Effects of Gut Microbiome of Black Soldier Fly Larvae (Hermetia illucens) on the Biodegradation of Food Waste*; Zhejiang University: Hangzhou, China, 2018. (In Chinese)
27. Wei, Z.C.; Su, G.L.; Li, X.Q.; Wang, F.M.; Sun, C.Z.; Meng, P.X. Parameter optimization and test of potato harvester wavy sieve based on edem. *Trans. Chin. Soc. Agric. Mach.* **2020**, *51*, 109–122. (In Chinese)
28. Liu, Y.C.; Zhang, F.W.; Song, X.F.; Wang, F.; Zhang, F.Y.; Li, X.Z.; Cao, X.Q. Study on mechanical properties for corn straw of double-layer bonding model based on discrete element method. *J. Northeast. Agric. Univ.* **2022**, *53*, 45–54. (In Chinese)
29. Dop, A.; Pac, B. A bonded-particle model for rock. *Int. J. Rock Mech. Min. Sci.* **2004**, *41*, 1329–1364.
30. Du, X.; Liu, C.L.; Jiang, M.; Yuan, H.; Dai, L.; Li, F.L. Calibration of bonding model parameters for coated fertilizer s based on discrete element method. *Trans. Chin. Soc. Agric. Mach.* **2022**, *53*, 141–149. (In Chinese)
31. Shen, H.H.; Zhang, H.; Fan, J.K.; Xv, R.Y.; Zhang, X.M. A rock modeling method of multi-parameters fitting in edem. *Rock Soil Mech.* **2021**, *42*, 2298–2310+2320. (In Chinese)
32. Zhang, Y.L. *Simulation and Experimental Study of Soil Throwing Performance of Reversing Rotary Tillage and Fertilizer Planter Based on Discrete Elements*; Jiangsu University: Zhenjiang, China, 2012. (In Chinese)
33. Shi, L.R.; Wu, J.M.; Zhao, W.Y.; Sun, W.; Zhang, F.W.; Sun, B.G. Establishment and parameter verification of farmland soil modelin uniaxial compression based on discrete element method. *J. China Agric. Univ.* **2015**, *20*, 174–182. (In Chinese)
34. Peng, C.W.; Zhou, T.; Song, S.S.; Fang, Q.; Zhu, H.Y.; Sun, S.L. Measurement and analysis of restitution coefficient of black soldier fly larvae in collision models based on hertz contact theory. *Trans. Chin. Soc. Agric. Mach.* **2021**, *52*, 125–134. (In Chinese)
35. Dong, K.; Esfandiary, A.H.; Yu, A. Discrete particle simulation of particle flow and separation on a vibrating screen: Effect of aperture shape. *Powder Technol.* **2016**, *314*, 195–202. [CrossRef]
36. Tao, G.X.; Zhang, Z.H.; Yi, S.J.; Xia, C.L.; Ma, Y.C. Design and test of combined swing radix isatidi root-soil separation device. *Trans. Chin. Soc. Agric. Mach.* **2022**, *53*, 109–119. (In Chinese)
37. Wei, Z.C.; Li, H.W.; Sun, C.Z.; Li, X.Q.; Su, G.L.; Liu, W.Z. Design and experiment of potato combined harvestor based on multi-stage separation technology. *Trans. Chin. Soc. Agric. Mach.* **2019**, *50*, 129–140. (In Chinese)
38. Lin, J.C.; Wang, D.M.; Yuan, J.; Li, G.X.; Li, Q.F.; Yuan, Q.X. Separation and harvest technology for earthworm-vermicompost and key component experiments. *Trans. Chin. Soc. Agric. Eng.* **2022**, *38*, 233–242. (In Chinese)